Wood Sci Technol (2007) 41:209–234
DOI 10.1007/s00226-006-0106-5

ORIGINAL

A global rheological model of wood cantilever as applied to wood drying

Mohssine Moutee · Yves Fortin · Mario Fafard

Received: 16 February 2006 / Published online: 26 October 2006

Abstract In the process of wood drying inevitable stresses are induced. This often leads to checking and undesired deformations that may greatly affect the quality of the dried product. The purpose of this study was to propose a new rheological model representation capable to predict the evolution of stresses and deformations in wood cantilever as applied to wood drying. The rheological model considers wood shrinkage, instantaneous stress–strain relationships, time induced creep, and mechano-sorptive creep. The constitutive law is based on an elasto–viscoplastic model that takes into account the moisture content gradient in wood, the effect of external load, and a threshold viscoplastic (permanent) strain which is dependent on stress level and time. The model was implemented into a numerical program that computes stresses and strains of wood cantilever under constant load for various moisture content conditions. The results indicate that linear and nonlinear creep behavior of wood cantilever under various load levels can be simulated using only one Kelvin element model in combination with a threshold-type viscoplastic element. The proposed rheological model was first developed for the identification of model parameters from cantilever creep tests, but it can be easily used to simulate drying stresses of a piece of wood subjected to no external load. It can therefore predict the stress reversal phenomenon, residual stresses and maximum stress through thickness during a typical drying process.

M. Moutee · Y. Fortin (✉)
Centre de recherche sur le bois (CRB),
Département des sciences du bois et de la forêt,
Université Laval, Québec, QC, Canada G1K 7P4
e-mail: mohssine.moutee.1@ulaval.ca
e-mail: Yves.Fortin@sbf.ulaval.ca

M. Fafard
Département de génie civil, Université Laval, Québec, QC, Canada G1K 7P4

Introduction

In the process of wood drying inevitable stresses are produced. The stress level depends on several factors such as the drying process, drying schedule, wood species, sawing pattern, and board thickness. Checking and undesired deformations are the most detrimental defects caused by drying stresses. If not properly relieved through conditioning, residual drying stresses may have a great impact on the quality of manufactured wood products. The detection or on-line monitoring of drying stresses in wood during drying is very difficult to perform in practice, even in closely controlled laboratory experiments. In order to avoid the formation of surface or internal checks in wood, the usual approach in commercial kilns is the use of conservative drying schedules that keep the drying stresses below the strength of the wood at any given temperature and moisture content. Unfortunately, this is generally done at the expense of time and energy and any modification to be brought to the drying schedule is a risky adventure. Therefore, there is a need for the development of predictive mathematical models describing the mechanism of stress development in wood during drying so as to build optimized drying schedules that can minimize drying stresses and deformations.

In order to analyze the mechanical behavior of wood during drying, it is important to understand the basic characteristics of heat and mass transfer in wood and their effect on stress development. The typical pattern of stress development during wood drying exhibits a state of tensile stresses at the board surface and compression stresses in the core at the beginning of drying, and vice versa at the end of drying. The stress reversal phenomenon occurs because in the early stages of drying a state of permanent or sub-permanent wood deformation takes place at the board surface (tension set) and in the interior zones. The mechanical behavior of wood is very complex, exhibiting immediate creep characteristics upon application of an external load or internal induced stress. This ''memory'' effect of wood has to be taken into account for a good understanding of the mechanical behavior of wood during drying. Another phenomenon that occurs when wood is subjected to both stresses and moisture losses is a complementary deformation known as mechano-sorptive (MS) deformation. This deformation is generally considered to be larger than the creep deformation occurring under constant moisture content conditions (Ranta-Maunus 1992; Mårtensson 1994; Dinwoodie et al. 1995; Wu and Milota 1995; Hanhijärvi 2000).

A number of rheological models of wood drying have been proposed during the last two decades (Rice and Youngs 1990; Salin 1992; Ranta-Maunus 1992, 1993; Svensson 1995, 1996; Wu and Milota 1995; Mårtensson and Svensson 1997; Ormarsson et al. 1999; Haque et al. 2000; Dahlblom et al. 2001; Pang 2001). Salin (1989) and Rice and Youngs (1990) mentioned that the Burger model used for describing viscoelastic strain could

not fully account for the observed stress levels in the timber. The Kelvin model, or *N* Kelvin associated elements model, has been the most commonly used mechanical analog to describe viscoelastic behavior in wood (Hanhijärvi 2000; Haque et al. 2000; Allegretti et al. 2003; Perré and Passard 2004). However, using *N* Kelvin elements model increases the number of rheological parameters that need to be computed, thus bringing more difficulty into the solution or more dispersion in the solved rheological parameter values. Furthermore, the determination of each group of parameters requires a different load level.

A few studies have been carried out on the effect of stress level on the creep properties of wood. It is generally thought that wood at low stress level is a linear viscoelastic material; otherwise, it is a nonlinear viscoelastic material. A nonlinearity of creep at about 50% of the bending strength and at about 70% of the maximum strength in compression was reported by Kingston and Budgen (1972). Miller and George (1974) observed that spruce wood in simple beam bending becomes a nonlinear viscoelastic material at a stress level of 40%. A similar study on four tropical hardwoods from Cameroon reported a nonlinear creep behavior in bending at a stress level as low as 35% (Foudjet and Bremond 1989).

It has often been asked whether the mechano-sorptive creep is an independent phenomenon, or whether the intensified creep is a result of high stresses caused by moisture gradients. In some rheological models, considering that viscoelastic creep at constant moisture content (MC) is negligible compared to the mechano-sorptive one, the viscoelastic creep component is deliberately omitted (Ranta-Maunus 1990; Ormarsson et al. 1999). However, the basic mechanism of mechano-sorption remains unclear and the diversity of experimental methods makes it difficult to compare published results. Despite the progress made during the last two decades in the development of mechanical models with respect to wood drying, there is still room for improvement, and much remains to be done in the determination of model parameters.

This paper presents a wood drying model based on classical rheology as applied to a cantilever specimen used to determine model parameters. The model exhibits the elastic behavior, the ''memory'' effect of wood (creep), the permanent deformation by introducing the concept of a ''threshold'' viscoplastic strain, the combined effect of drying rate and load (mechano-sorptive strain), and the free shrinkage strain. The main originality of the proposed rheological model is that it takes into account any non linear viscoelastic behavior of the wood cantilever. The material properties are assumed to be affected by moisture content and temperature variations during drying. The rheological model is implemented into an applicable program that simulates the creep of a cantilever loaded at free end under constant moisture content conditions and under drying conditions (Moutee et al. 2005). The effect of viscoelastic creep and the effect of mechano-sorptive creep are first considered separately, and then where both are effective.

Background theory

Cantilever equilibrium equations

The creep modeling approach is based on the theory of a cantilever subjected to a punctual load at free end in which the moisture content effect on stress distribution is taken into account. The mathematical development of the cantilever theory is given in Moutee et al. (2005). Only the main strain and stress equations will therefore be recalled here. Considering an orthotropic wood cantilever beam with dimensions l:length × b:width × h:thickness (Fig. 1a), the total strain distribution at coordinate x is, according to the Euler-Bernoulli assumption, linear through the thickness (Fig. 1b):

$$\varepsilon(z) = \varepsilon_{\mathrm{uf}} \times \frac{z - z_0}{(h/2) - z_0} \tag{1}$$

where $\varepsilon_{\mathrm{uf}}$ is the strain at surface layer $z = h/2$ and z_0 is the position of the neutral axis (where the total strain is zero) relative to the geometric axis.

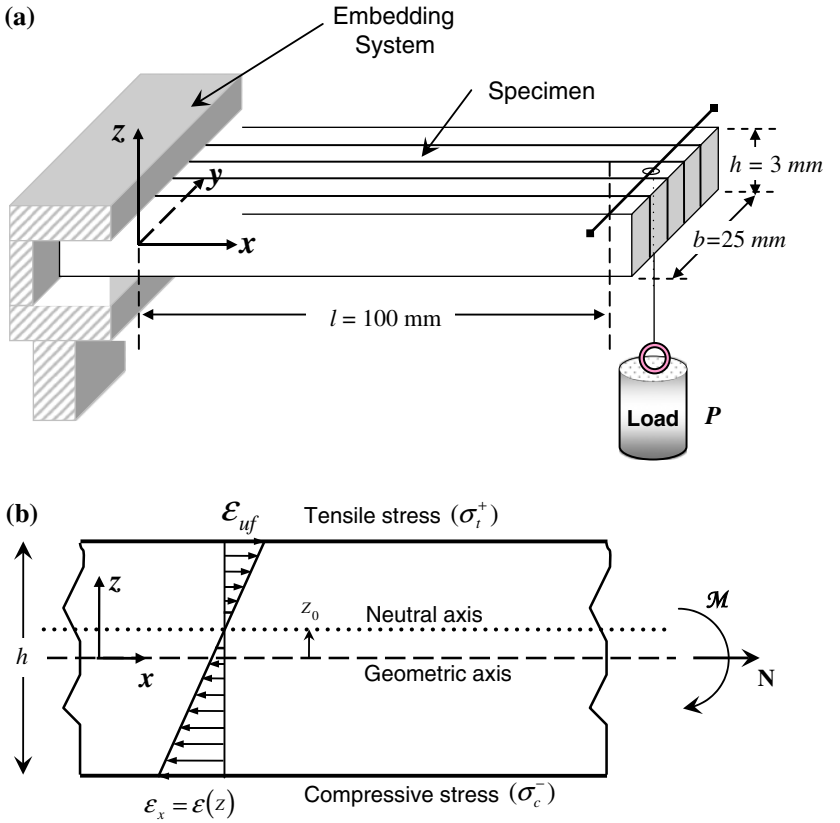

Fig. 1 **a** Wood cantilever. **b** Schematic of strain distribution through cantilever thickness (xz-plan) at x position (z_0 is the neutral axis location)

There are two unknown variables (ε_{uf} and z_0), meaning that two equations are required to determine the two values. The equilibrium equations of cantilever beam theory are

$$R_{\mathcal{M}} \equiv b \cdot \int_{-h/2}^{h/2} \sigma(x,z) \cdot (z - z_0)\, \mathrm{d}z - \mathcal{M}(x) = 0 \tag{2a}$$

$$R_N \equiv b \cdot \int_{-h/2}^{h/2} \sigma(x,z)\, \mathrm{d}z = 0 \tag{2b}$$

where σ is the stress distribution through the thickness, z_0 is the position of the neutral axis and $\mathcal{M} = P(l - x)$ is the bending moment at coordinate x due to the applied load P. In the absence of an axial load, the load P will induce tensile stresses σ_t^+ in all fibers lying on the positive side of the neutral axis, and compressive stresses σ_c^- in all fibers beneath the neutral axis (Fig. 1b).

Substituting into Eqs. 2a, 2b, the strain–stress relation of the rheological constitutive model, the stress field at the given location in time and space (t,x,z) can be easily estimated. No assumption is needed on the stress distribution through the thickness. For a given time t and for a given position x, the values of ε_{uf} and z_0 are computed through an iterative procedure and then the stress field through the beam thickness. The curvature of the cantilever is given by

$$\chi(x,t) = \frac{\varepsilon_{uf}(x,t)}{(h/2) - z_0(x,t)} \tag{3}$$

and the deflection by

$$w(x,t) = \int_0^x \int_0^x \chi(u,t)\mathrm{d}u \tag{4}$$

For the modeling of induced drying stresses only, the cantilever is free of load and the bending moment $\mathcal{M}$ of Eq. 2a is set equal to zero.

Rheological model

Rheological processes in wood are very complex, and care must be taken to avoid oversimplification. However, the various phenomena in the rheological processes can be described fairly accurately through a combination of spring and viscous dashpot elements. Under constant moisture content conditions

the mechanical behavior of wood is usually assumed to be viscoelastic. Models of pure viscoelastic creep in wood often consist of series or parallel combinations of spring and dashpot elements, such as the Maxwell and Kelvin models. In the Burger model, a Maxwell and a Kelvin model are connected in series. Purely mathematical power-law expressions are also used to fit creep data (Haque et al. 2000).

Global hygro-mechanical constitutive model

In situation of isothermal drying and in uniaxial rheological behavior, the total strain is composed of the elastic strain (ε_e), viscoelastic strain (ε_v) (totally recoverable), ''viscoplastic'' strain (ε_p) (permanent deformation), and mechano-sorptive strain (ε_{ms}), in addition to the deformation due to free shrinkage (ε_M) (Fig. 2):

$$\varepsilon = \varepsilon_e + \varepsilon_v + \varepsilon_p + \varepsilon_{ms} + \varepsilon_M \tag{5}$$

The arrows in Fig. 2 represent the direct effect of drying on wood mechanical behavior. A rate formulation of Eq. 5 is more convenient for the mathematical representation of these mechanical phenomena. The total strain rate formulation can be written as

$$\dot{\varepsilon} = \dot{\varepsilon}_e + \dot{\varepsilon}_v + \dot{\varepsilon}_p + \dot{\varepsilon}_{ms} + \dot{\varepsilon}_M \tag{6}$$

where the overdot represents the time derivative. Mathematical modeling of internal stress development in wood during drying requires detailed knowledge about each strain component. Each strain component is developed hereinafter in one-dimensional formulation.

Instantaneous strain rate is related to stress rate by

$$\dot{\varepsilon}_e = \frac{d}{dt}\left(\frac{\sigma}{E_e}\right) \tag{7}$$

where σ is the applied stress (or drying stress), and E_e the Hookean spring constant (Young's modulus).

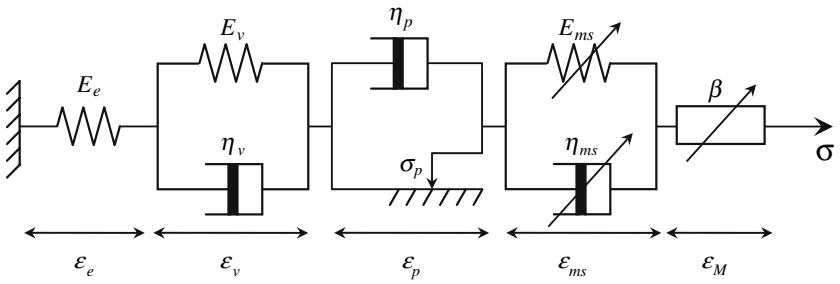

Fig. 2 Schematic representation of the proposed rheological model

Kelvin model is used to represent the total recoverable strain after unloading. The viscoelastic stress–strain relationship is given by

$$\sigma = E_v \cdot \varepsilon_v + \eta_v \cdot \dot{\varepsilon}_v \tag{8}$$

where σ is the applied stress, E_v and η_v the Hookean spring constant and viscosity of the Newtonian dashpot of the Kelvin element, respectively.

The viscoplastic strain is the permanent strain component of creep strain. The viscoplastic component is based on the Bingham model (Bingham 1922) where the viscoplastic stress–strain relationship is given by

$$\dot{\varepsilon}_{\mathrm{p}} = \frac{\mathrm{d}\varepsilon_{\mathrm{p}}}{\mathrm{d}t} = \begin{cases} 0 & \text{if } \sigma \leq \sigma_{\mathrm{p}} \\ \frac{1-\frac{\sigma_{\mathrm{p}}}{|\sigma|}}{\eta_{\mathrm{p}}}\sigma & \text{if } |\sigma| > \sigma_{\mathrm{p}} \end{cases} \tag{9}$$

where η_{p} is the viscosity of the Newtonian dashpot associated with unrecoverable strain.

The mechano-sorptive effect starts to take place below fiber saturation point (FSP), and occurs as soon as the moisture content changes during drying. The proposed mechano-sorptive model is the one presented by Salin (1992):

$$\dot{\varepsilon}_{\mathrm{ms}} = \frac{\mathrm{d}\varepsilon_{\mathrm{ms}}}{\mathrm{d}t} = \frac{1}{\eta_{\mathrm{ms}}}\left|\frac{\mathrm{d}M}{\mathrm{d}t}\right|(\sigma - E_{\mathrm{ms}} \cdot \varepsilon_{\mathrm{ms}}) \tag{10}$$

where $\frac{1}{\eta_{\mathrm{ms}}}$ is the mechano-sorptive coefficient (MPa^{-1}), E_{ms} the apparent mechano-sorptive modulus, and $\left|\frac{\mathrm{d}M}{\mathrm{d}t}\right|$ is the absolute value of the drying rate.

From Eq. 10, we have

$$\sigma = \eta_{\mathrm{ms}}\frac{1}{|\mathrm{d}M/\mathrm{d}t|}\dot{\varepsilon}_{\mathrm{ms}} + E_{\mathrm{ms}}\,\varepsilon_{\mathrm{ms}} \tag{11}$$

This equation is analogous to the Kelvin model for viscoelastic creep (Eq. 8) except for the change of the variable ''time'' t for ''moisture content'' M, the effect of time being implicitly taken into account in the value of M. The material constants describing the interaction of stress and moisture change are assumed to be independent of stress for the specified sorption and loading conditions (Wu and Milota 1996).

Shrinkage appears in all parts of the board for which the MC is within the hygroscopic range:

$$\dot{\varepsilon}_M = \frac{\mathrm{d}\varepsilon_M}{\mathrm{d}t} = \beta \cdot \left.\frac{\mathrm{d}M}{\mathrm{d}t}\right|_{M \leq \mathrm{FSP}} \tag{12}$$

where β is the shrinkage/swelling coefficient (independent of moisture) and $\frac{\mathrm{d}M}{\mathrm{d}t}$ is the drying rate below FSP.

The model of Fig. 2, which describes uniaxial behavior only, consists of eight unknown parameters. The model can be expanded for two-dimensional or

three-dimensional studies. In the three-dimensional case and considering orthotropy of wood, we need a fourth order tensor for each parameter, except for shrinkage that needs second order tensor (Moutee et al. 2002).

Global model decomposition and simulation considerations

In order to exhibit the behavior of each component and their relative importance in the proposed global rheological model, various combinations of the model parameters (Table 1) were considered separately using the cantilever as loading mode.

Elasto–viscoplastic model in constant hygrothermal conditions (Model 1)

For the elasto–viscoplastic model (i.e., the three first components of global rheological model of Fig. 2), if stresses developed in the material upon application of the load are smaller than the threshold stress, the deformation of the body can be divided into instantaneous elastic and delayed elastic components (viscoelastic creep). The instantaneous elastic and delayed elastic deformations are totally recoverable on removal of load, providing the delayed elastic deformation is allowed sufficient time. If the applied load causes stresses that exceed the threshold stress (high stress level), permanent deformation will take place immediately, and later, after unloading, the deformation will not be totally recoverable. The magnitude of the non recoverable strain depends on applied load level and time.

For a cantilever, the maximum stress is located at the surface (tensile stress at the upper face and compressive stress at lower face) and the zero stress is located at mid-thickness (neutral axis). If the stress at surface is above the threshold, this means that somewhere in the cantilever thickness the stress is under the threshold and a nonlinear stress pattern develops (Fig. 3). Model 1 is therefore adequate to simulate creep and creep recovery both at low and high stress levels.

Elasto–viscoplastic model in drying conditions (Model 2)

For stress modeling in drying conditions, the shrinkage component is added to Model 1 to give Model 2. This combination is further complicated by the fact

Table 1 Alternative models

Material assumption	Elastic strain	Recoverable strain	Unrecoverable strain	Shrinkage strain	Mechano-sorptive strain
Model 1	$\dot{\varepsilon}_{\mathrm{e}}$	$\dot{\varepsilon}_{v}$	$\dot{\varepsilon}_{\mathrm{p}}$		
Model 2	$\dot{\varepsilon}_{\mathrm{e}}$	$\dot{\varepsilon}_{v}$	$\dot{\varepsilon}_{\mathrm{p}}$	$\dot{\varepsilon}_{M}$	
Model 3	$\dot{\varepsilon}_{\mathrm{e}}$	$\dot{\varepsilon}_{v}$	$\dot{\varepsilon}_{\mathrm{p}}$	$\dot{\varepsilon}_{M}$	$\dot{\varepsilon}_{\mathrm{ms}}$

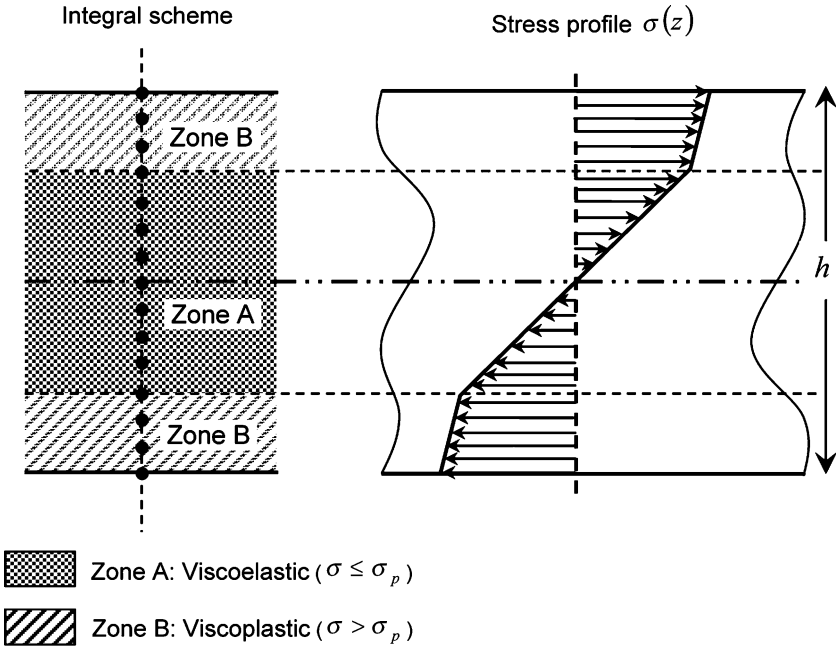

Fig. 3 Localization of plastic threshold through board thickness in numerical procedure and the resulting nonlinear stress profile

that the elastic and creep parameters vary with time since they are moisture content dependent. Model 2 is used hereinafter for stress pattern calculation in isothermal drying conditions under load, and without load (real drying).

Global rheological model (Model 3)

Model 3 represents the global rheological model described previously. Model 2 describes the effect of viscoelastic creep behavior only. By adding the mechano-sorptive component, Model 3 allows us to simulate the overall effect of drying on stress development in wood. The study of various combinations of the proposed global model is useful for the elaboration of an experimental setup that makes easier the step by step determination of global rheological model parameters. This also exhibits the consequence on drying stress patterns of considering the viscoelastic creep and the mechano-sorptive creep either separately or together.

Moisture content effects on model parameters

In drying conditions, mechanical properties of wood are affected by moisture content and temperature changes. Therefore, the parameters of rheological

model must be adjusted for their hygrothermal state. However, the temperature effect was not considered in this study. The elastic modulus dependency on moisture content was based on the formulation proposed by Guitard (1987). As no information was available for the moisture content effect on viscous parameters, we assumed that the elastic formulation was applicable:

$$E_i^M = E_i^{12}[1 - 0.015(M - 12)] \tag{13}$$

$$\eta_j^M = \eta_j^{12}[1 - 0.015(M - 12)] \tag{14}$$

where E_i^M is the elastic modulus at the actual MC ($i = e,v$); E_i^{12} is the elastic modulus at 12% MC; η_j^M is the viscous coefficient at the actual MC ($j = v,p$); and η_j^{12} is the viscous coefficient at 12% MC. Equations 13 and 14 are valid for moisture content between 6% and FSP. In this study, we consider that the mechano-sorptive coefficients (E_{ms} and η_{ms}) are not affected by moisture content change as no published data seem to be available on the subject.

Moisture content gradient development

This paper is not aimed at modeling the heat and mass transfer in wood during drying. However, for the application of the proposed rheological model in drying conditions, we need a one dimensional water transport history to be used as input for drying stress–strain simulation. Thus, a numerical algorithm was built to reproduce moisture content profiles representative of a conventional drying program:

$$M(z,t) = a(t)z^3 + b(t)z^2 + c(t)z + d(t)$$

where $a(t)$,$b(t)$,$c(t)$, and $d(t)$ are second order polynomial function of time.

Figure 4 shows the evolution of the moisture content profiles over thickness. The total drying time from 40% to 10% MC was assumed to be 8 h for a longitudinally oriented 3-mm thick cantilever (Fig. 1).

Numerical procedure

For the numerical simulation of creep and creep recovery of wood under load, the global model has to be implemented into a computer program. The implemented model is nonlinear and the description of the development of stresses and strains is history dependent. Therefore, an implicit integration scheme technique is used to reduce numerical errors introduced in each time step, and to perform iterations of the solution during each time increment. Note that, in this section, only the numerical procedure of the global mathematical model is presented. The same formulation technique is used for all alternative models presented in Table 1.

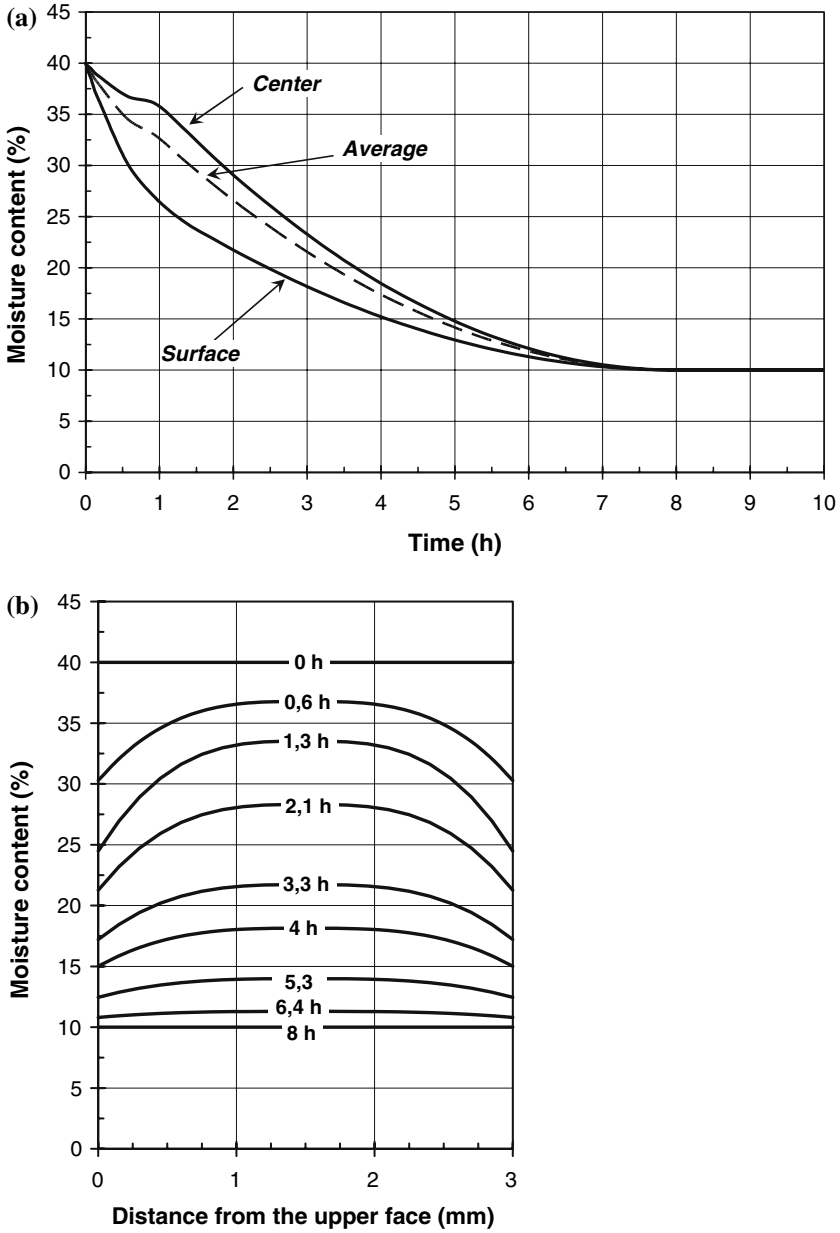

Fig. 4 Moisture content evolution with time. **a** Center, surface and average moisture content. **b** Moisture content profiles through thickness at different drying times

For the implementation of the numerical procedure, Eqs. 5–11 must be rewritten into stress formulation at position x and z of a cantilever beam subjected to a single load P at the free end. Equation 5 can be rewritten as

$$\sigma = E_e \cdot (\varepsilon - \varepsilon_v - \varepsilon_p - \varepsilon_{ms} - \varepsilon_M) \tag{15}$$

Substituting Eq. 15 into Eqs. 8, 9 and 11, we obtain

$$\begin{cases} \eta_v \dot{\varepsilon}_v + (E_e + E_v) \cdot \varepsilon_v + E_e \cdot \varepsilon_p + E_e \cdot \varepsilon_{ms} = E_e \cdot (\varepsilon - \varepsilon_M) \\ \eta_p \dot{\varepsilon}_p + E_e \varepsilon_p + E_e \varepsilon_v + E_e \cdot \varepsilon_{ms} = E_e \cdot (\varepsilon - \varepsilon_M) - \text{sign}(\sigma) \cdot \sigma_p \\ \frac{\eta_{ms}}{|\dot{M}|} \cdot \dot{\varepsilon}_{ms} + E_e \varepsilon_v + E_e \varepsilon_p + (E_e + E_{ms}) \cdot \varepsilon_{ms} = E_e \cdot (\varepsilon - \varepsilon_M) \end{cases} \tag{16}$$

where $\text{sign}(\sigma) = \frac{\sigma}{|\sigma|} = \begin{cases} +1 & \text{if } \sigma > 0 \\ -1 & \text{if } \sigma < 0 \end{cases}$

In matrix notation we have

$$\begin{bmatrix} \eta_v & 0 & 0 \\ 0 & \eta_p & 0 \\ 0 & 0 & \frac{\eta_{ms}}{|\dot{M}|} \end{bmatrix} \begin{Bmatrix} \dot{\varepsilon}_v \\ \dot{\varepsilon}_p \\ \dot{\varepsilon}_{ms} \end{Bmatrix} + \begin{bmatrix} E_e + E_v & E_e & E_e \\ E_e & E_e & E_e \\ E_e & E_e & E_e + E_{ms} \end{bmatrix} \begin{Bmatrix} \varepsilon_v \\ \varepsilon_p \\ \varepsilon_{ms} \end{Bmatrix} = \begin{Bmatrix} E_e \cdot (\varepsilon - \varepsilon_M) \\ E_e \cdot (\varepsilon - \varepsilon_M) \\ E_e \cdot (\varepsilon - \varepsilon_M) \end{Bmatrix} - \text{sign}(\sigma) \begin{Bmatrix} 0 \\ \sigma_p \\ 0 \end{Bmatrix} \tag{17}$$

Using an implicit integration scheme, Eq. 17 becomes

$$[A]^{k+1} \begin{Bmatrix} \varepsilon_v \\ \varepsilon_p \\ \varepsilon_{ms} \end{Bmatrix}^{k+1} = [B]^{k+1} \begin{Bmatrix} \varepsilon_v \\ \varepsilon_p \\ \varepsilon_{ms} \end{Bmatrix}^{k} + \begin{Bmatrix} 1 \\ 1 \\ 1 \end{Bmatrix} E_e^{k+1} \cdot (\varepsilon^{k+1} - \varepsilon_M^{k+1}) - \text{sign}(\sigma) \begin{Bmatrix} 0 \\ \sigma_p \\ 0 \end{Bmatrix}^{k+1} \tag{18}$$

where

$$[A] = \begin{bmatrix} \frac{\eta_v}{\Delta t} + (E_e + E_v) & E_e & E_e \\ E_e & \frac{\eta_p}{\Delta t} + E_e & E_e \\ E_e & E_e & \frac{\eta_{ms}}{|\Delta M|} + E_e + E_{ms} \end{bmatrix}; \quad [B] = \begin{bmatrix} \frac{\eta_v}{\Delta t} & 0 & 0 \\ 0 & \frac{\eta_p}{\Delta t} & 0 \\ 0 & 0 & \frac{\eta_{ms}}{|\Delta M|} \end{bmatrix}$$

Matrices $[A]$ and $[B]$ represent material parameters which are evaluated at time $k + 1$ using Eqs. 13 and 14, except for the mechano-sorptive coefficient (E_{ms} and η_{ms}). The numerical solution of Eq. 18 was obtained using the ''LinearSolve'' command in Maple Enginering Software.

By dividing the board into n-layers of equal thickness and using linearization technique where iterations are made for each time step until equilibrium is reached, the strain field $\varepsilon(z)$ and stress field $\sigma(z)$ are simultaneously computed at (x,z) position. Thus the deflection at any position x of the beam length (Eq. 4) can be obtained. The developed numerical procedure is able to locate where the threshold stress is reached into the thickness.

Material data

The material parameters used for the simulations are assumed to be representative of white spruce (*Picea glauca* (Moench.) Voss.) wood in the longitudinal direction at a temperature of 60°C and at 12% MC: E_e = 6,200 MPa, E_v = 40,450 MPa, η_v = 52,834 MPa.h, η_p = 40,510 MPa.h, E_{ms} = 2,000 MPa and η_{ms} = 1,000 MPa. These parameters were inferred from experimental creep data obtained on a cantilever of 100 mm span (longitudinal direction), 25 mm width and 3 mm thickness (Fortin et al. 1999). Longitudinal shrinkage was assumed to be linear with a total shrinkage coefficient β = 0.3%. The threshold value of viscoplastic strain was assumed to correspond to 30% of the bending strength. As the bending strength is affected by moisture content, obtained from experimental investigation, the threshold value was evaluated at actual moisture content during drying (Fig. 5).

Results and discussion

Load level effects in constant hygrothermal conditions (Model 1)

The first simulation consists in modeling the creep in constant hygrothermal conditions (MC = 15%; T = 60°C) under three various constant stress levels calculated at the cantilever fixed-end. The stress levels (SL) are 30, 50 and 70% of bending strength, the corresponding load being 500, 835 and 1170 g, respectively. The results are analyzed at quarter span (x = l/4) for a loading

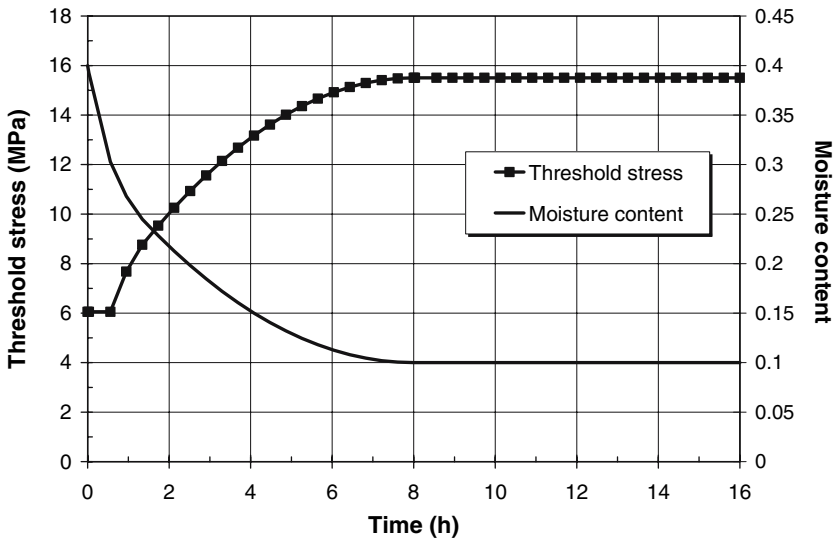

Fig. 5 Viscoplastic threshold stress and moisture content as a function of time during drying and relaxing phase

time of 8 h. The same time period is used for the recovery part. The threshold stress value (30% of the bending strength) is 13.1 MPa.

Figure 6a shows the computed tensile stress at the upper fiber located at $x = l/4$ of cantilever length. It can be seen that for a constant load less than or equal to the viscoplastic threshold, the stress is constant during the loading

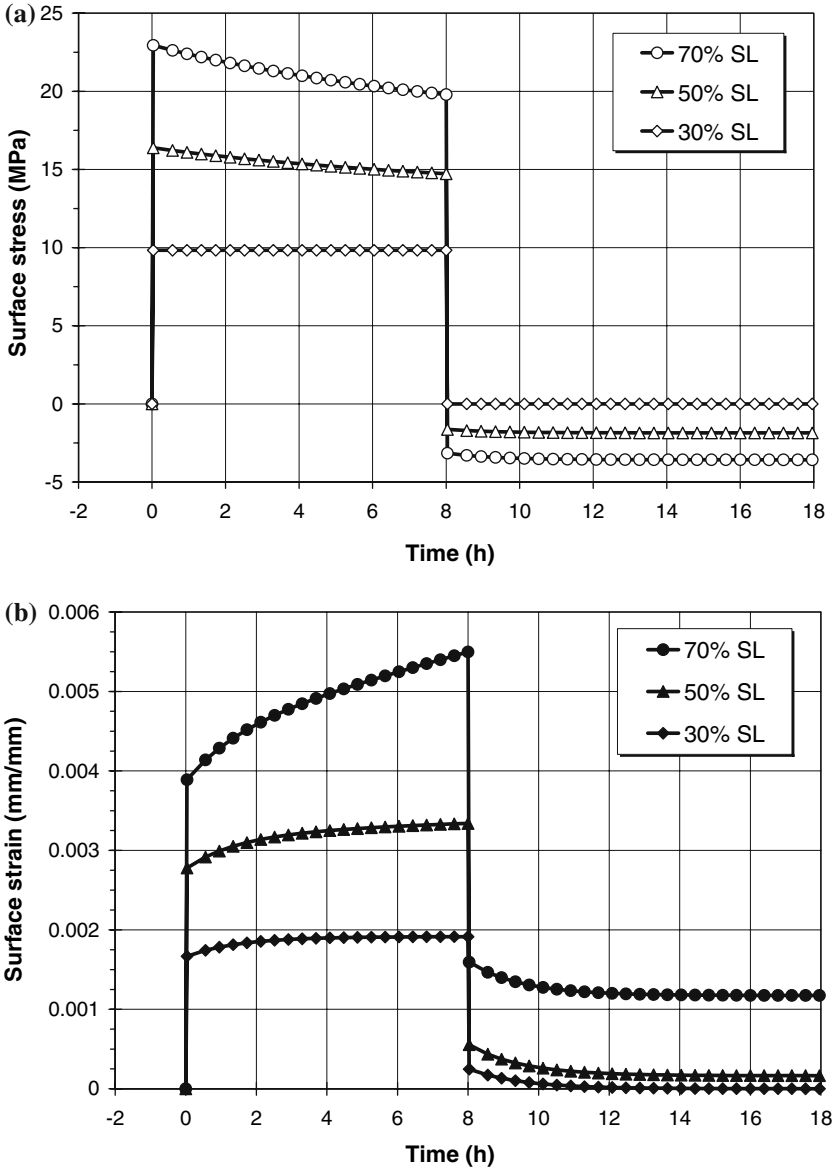

Fig. 6 Evolution of stress and tensile surface creep/recovery creep at $x = l/4$ for three stress levels at 15% MC (cantilever unloaded after 8 h). **a** Surface stress. **b** Surface strain

period and becomes null after unloading. However, this is not the case when the stress level is above the viscoplastic threshold. In such condition, even when the cantilever is under constant load, the stress decreases during loading time and a residual stress remains in wood after unloading. This phenomenon is well known in plastic behavior of beams (Shames and Cozzarelli 1992). Thus, in the presence of a viscoplastic threshold, the usual classical elastic beam theory used for the evaluation of stresses induced by a constant load is not correct for creep studies at high load level. The strain-time evolutions of Fig. 6b reflect the well known creep and creep recovery curves of wood material under load and after unloading. As expected, total surface creep increases with increasing stress level. It can also be observed that as long as the viscoplastic threshold is not reached, creep deformation is totally recoverable after unloading. However, when the load level is above the viscoplastic threshold, creep deformation is unrecoverable after unloading and its magnitude depends on stress level and loading time.

Figure 7a and b shows the stress profile through cantilever thickness at $x = l/4$ after 8 h of loading and 8 h after removal of the load, respectively. It can be seen that the stress distribution through thickness (Fig. 7a) is linear at ''low'' stress level (≤ 30%SL). However, at ''high'' stress level, the stress pattern through thickness is nonlinear, and after unloading residual stresses are present in the cantilever (Fig. 7b). Residual stresses at the upper face ($h = +1.5$ mm) are in compression and those at the lower face ($h = -1.5$ mm) are in tension. The latter phenomenon can be explained by the fact that when the cantilever is loaded above the threshold stress level (Fig. 6a), the first layers close to the upper and bottom faces undergo viscoplastic behavior, thus inducing permanent deformations. Fibers located at the upper face show positive permanent deformations and those at the bottom face, negative permanent deformations. The inner layers remaining viscoelastic, no permanent deformations are induced. After unloading, the inner layers tend to return to their initial position, but the external fibers having been permanently deformed restrain the movement, which in turn induces compressive stresses at the top face and tensile stresses at the bottom face.

For an experimental point of view, deflection measurement of cantilever is generally much easier to conduct than surface deformation measurement, especially at high temperature and high relative humidity conditions. Figure 8 shows the computation of the time dependent deflection at free end ($x = l$) of the cantilever. Of course, the deflection curve exhibits a similar shape as the surface deformation curve (Fig. 6b) since the deflection is inferred from axial deformation. This theoretical equivalence would have, however, to be verified by laboratory tests before limiting the measurements to free end deflection.

Figure 9 shows the computed stress versus the classical evaluation of stress using elastic beam theory equation $\left(\sigma(x) = \frac{h \cdot P(l-x)}{2I_z}\right)$ along the beam length after 8 h of constant load. It can be seen that the classical elastic beam theory overestimates for the first half of the cantilever span the induced stress due to applied bending load once the viscoplastic threshold is reached. It can

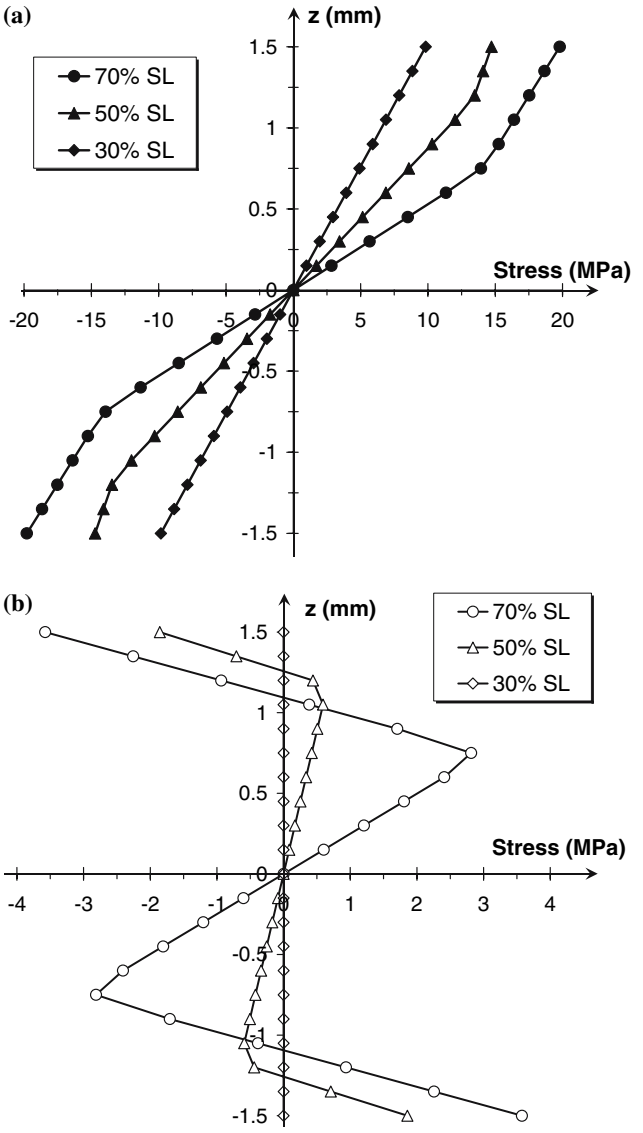

Fig. 7 Computed stress profile through thickness at $x = l/4$ for three stress levels at 15% MC. **a** Under load (at 8 h). **b** After relaxation (at 16 h)

therefore be erroneous to identify viscous parameters from laboratory tests when stress estimation is based on elastic beam theory.

Stress and strain in a cantilever loaded at free end during drying (Models 2 and 3)

The next simulations show the stress and strain evolution in a cantilever loaded at free end during drying. In order to examine the mechano-sorptive

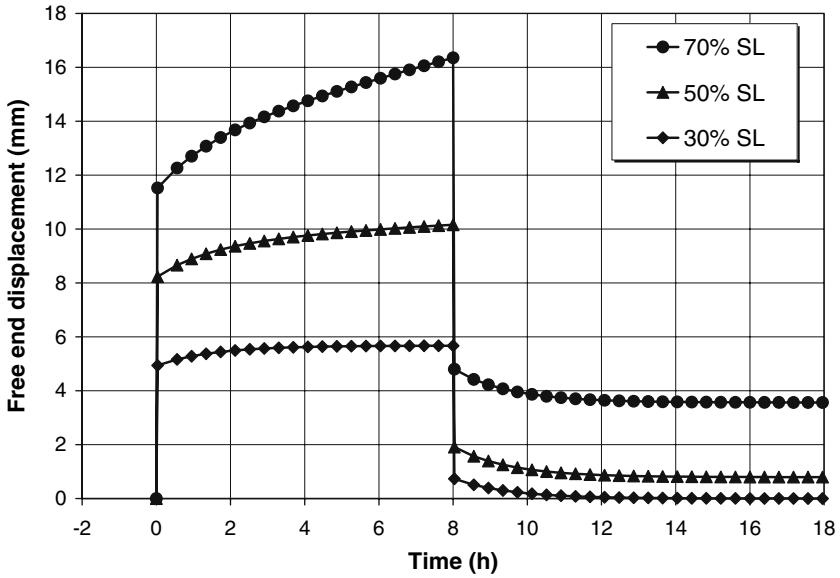

Fig. 8 Computed deflection at free end ($x = l$) for three stress levels at 15% MC

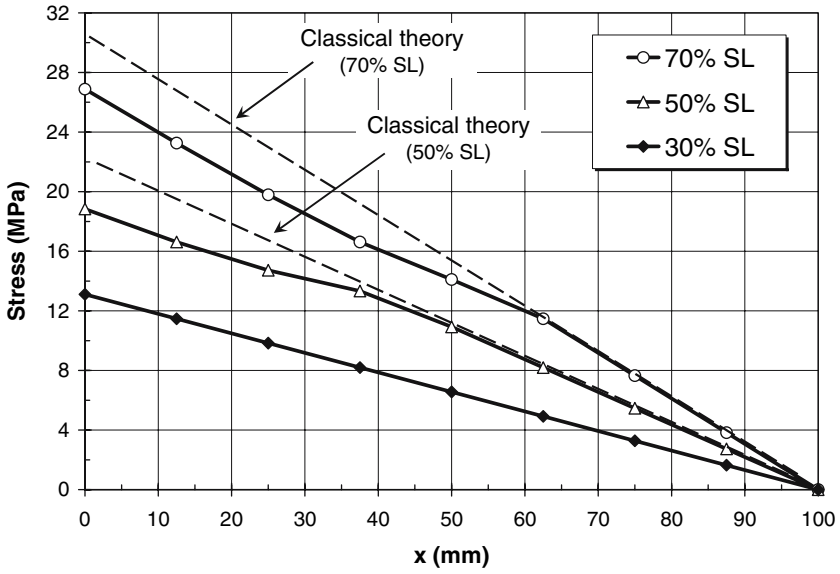

Fig. 9 Computed stress along the cantilever span versus stress based on bending classical theory (*dashed line*) for three stress levels at 15% MC (after 8 h of loading)

effect on the behavior of the cantilever, simulations were run without (Model 2) and with (Model 3) the rheological mechanism representing the mechano-sorptive behavior. The moisture content history imposed for these simulations is given in Fig. 4. The load imposed at free end was equal to 554 g, which

corresponds to a stress level of 70%. The shrinkage due to drying was supposed to be initiated at 30% MC.

The mechanical behavior of the cantilever without taking into account the mechano-sorptive mechanism is shown in Fig. 10. As we can see, except for the first one-half hour where the MC is above FSP the top and bottom fibers exhibit a different behavior both for the evolution of stress (Fig. 10a) and deformation (Fig. 10b). Immediately after the application of the load, the stress reaches a value of 10.9 MPa, which is above the viscoplastic threshold. The moisture content at the two faces drops below FSP (Fig. 4) after the first half-hour and shrinkage starts to take place, inducing tensile stresses in the surface layers and compressive stresses in the core. This leads within the first two hours of drying to an increase of the tensile stress at the top surface, up to a maximum of 13.8 MPa, and to a decrease of the compressive stress at the bottom surface, down to 8.9 MPa. These trends are reversed after two hours, which point corresponds to the beginning of the stress reversal phenomenon. The moisture content is then about 21% and the corresponding threshold stress is 9.8 MPa (Fig. 5). This means that the stress at the top surface is well above the plasticity limit (Fig. 5), whereas the stress at the bottom surface is below that limit.

At the end of drying (8 h), the stress at the top surface has decreased to 9.6 MPa and the stress at the bottom surface has increased to 10.9 MPa. This can be explained by the stress reversal phenomenon which contributes to decrease the stress on the tensile face and to increase it on the compressive face. After the load is removed, the top fiber undergoes a permanent residual compressive stress of about 1.3 MPa and the bottom fiber returns to almost zero stress. This is a direct result of the higher plastic deformation on the top fiber, which after unloading causes a higher residual stress.

In terms of deformation (Fig. 10b), the shrinkage under load decreases the total deformation of the tensile top surface and increases that of the compressive bottom surface. After unloading and relaxing (16 h), the total deformation on the top surface is slightly smaller than free shrinkage and vice versa for the total deformation on the bottom surface. This is caused by the differences in plastic deformation on the cantilever faces in the beginning of drying.

Figure 10c shows the stress distribution through thickness under load at the end of drying and after unloading and relaxing (16 h). We can see that the stress distribution through thickness at 8 h is nonlinear. At 16 h, the residual stress profile is highly non symmetrical with respect to the geometrical axis. It is obvious that this behavior is due to the drying induced stresses when we compare Fig. 10c with Fig. 7b which represents the residual stress profile under constant moisture content conditions. Despite that, these stress distributions satisfy the two equilibrium equations presented at Eqs. 2a and 2b.

Figure 11 reproduces the previous simulation except that we added the mechano-sorptive mechanism (Model 3). The results show the same trend as the previous simulation with Model 2, but as expected the mechano-sorptive effect has decreased the maximum stress for both the top surface

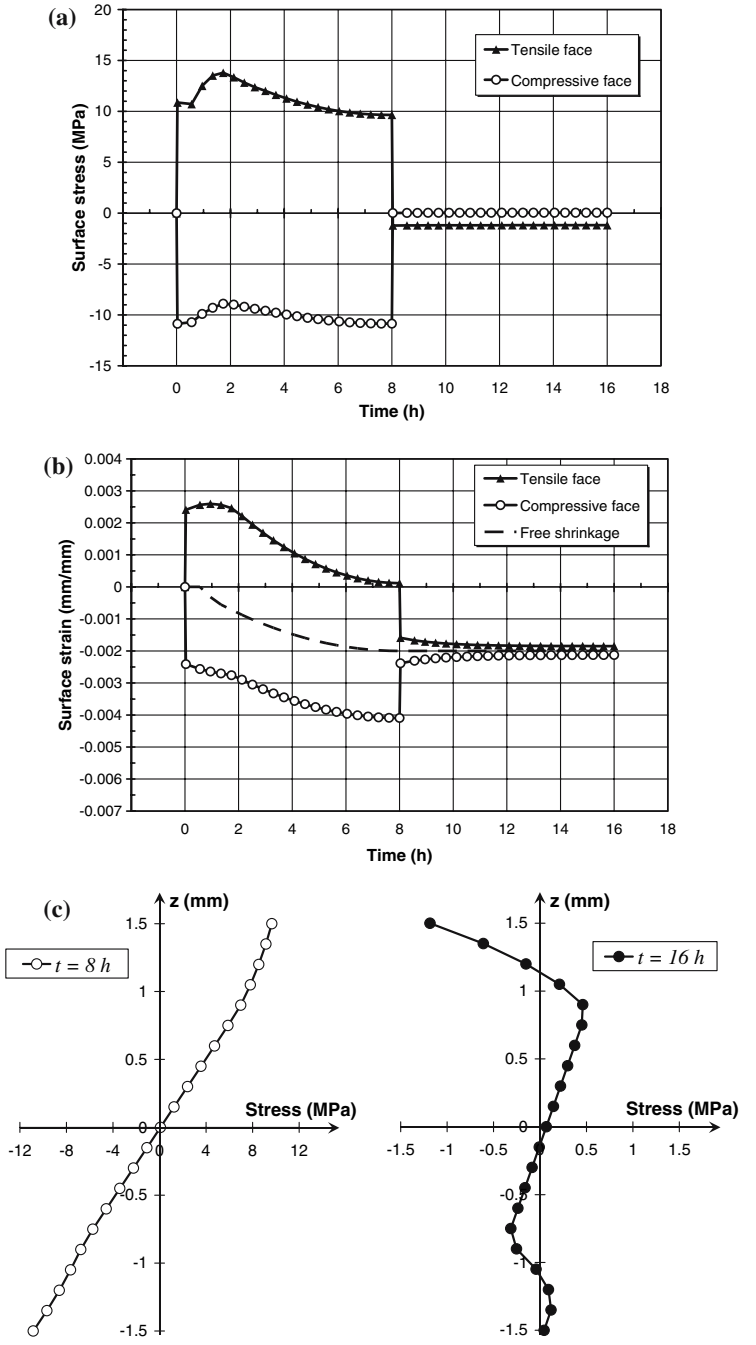

Fig. 10 Simulation results with Model 2 as applied to a cantilever at $x = l/4$ under 70% SL during drying and after unloading. **a** Surface stress. **b** Surface strain. **c** Stress profile through thickness at 8 h (loaded) and 16 h (unloaded)

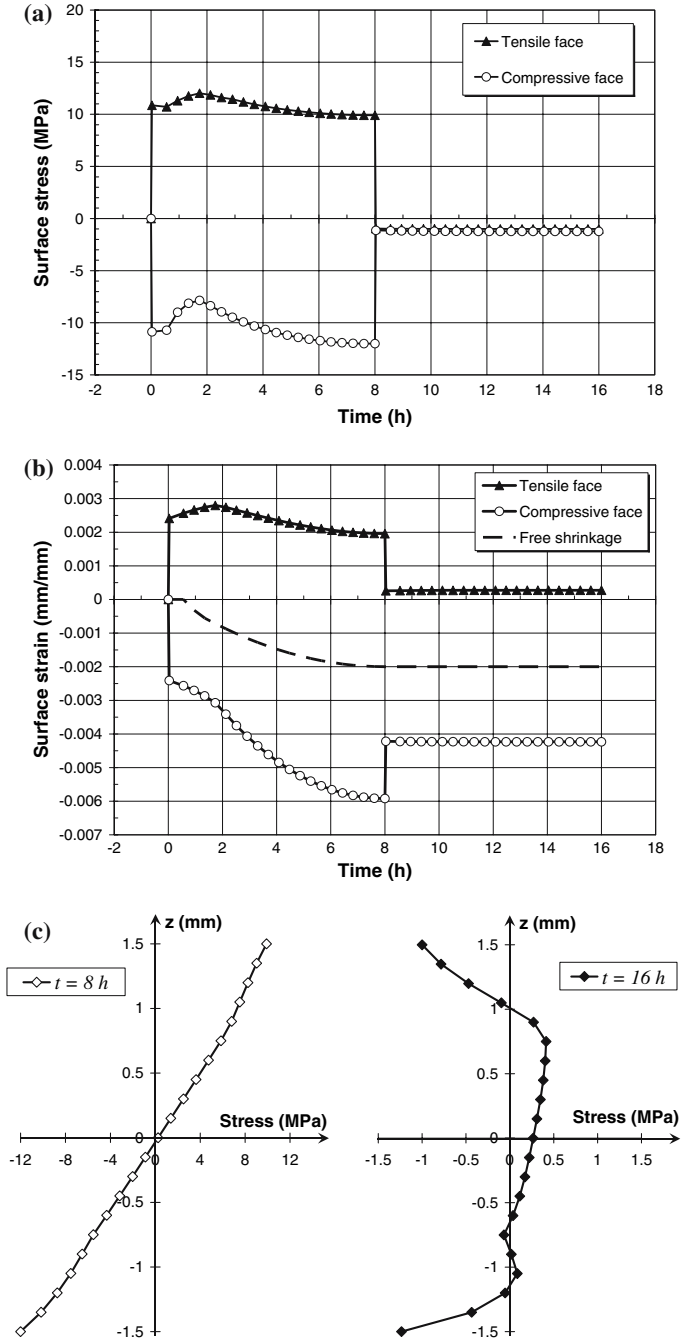

Fig. 11 Simulation results with Model 3 as applied to a cantilever at $x = l/4$ under 70% SL during drying and after unloading. **a** Surface stress. **b** Surface strain. **c** Stress profile through thickness at 8 h (loaded) and 16 h (unloaded)

(13.8–12.0 MPa) and bottom surface (8.9–7.8 MPa) (Fig. 11a) in the first stage of drying. However, at the end of drying, just before load removal, the stress level is slightly higher than it was for Model 2. This is explained by the complementary mechano-sorptive deformation in the beginning of drying. After unloading and relaxing, the two surfaces show non negligible residual stresses.

The mechano-sorptive behavior has an interesting effect on the evolution of the total deformation (Fig. 11b). In tension, the MS deformation has almost cancelled the shrinkage deformation, as it can be observed when comparing Fig. 11b with Fig. 10b. In compression, the MS deformation increases the total deformation (– 0.004 to – 0.006) since it is of the same sign as shrinkage deformation. Moreover, this is reflected in the residual deformation observed after unloading and relaxing.

Figure 11c shows the stress distribution through thickness at 8 and 16 h. The stress distribution after 8 h is nearly the same as the one observed for Model 2 (Fig. 10c) except for the bottom surface where the stress is slightly higher. After 16 h, the residual stresses on both the top and bottom surfaces are in this case in compression. The fact that the MS induced stress is more important than the residual viscoplastic load induced stress explains why the bottom face becomes in compression.

Drying stress without load (real drying)

Another simulation was done to study the stress evolution in the cantilever during drying without any external load. This represents a real drying case where the stresses are only induced by the variation of moisture content. The moisture content history used in this simulation was the same as the one used in previous simulations (Fig. 4). Here again, the drying time is 8 h and the total simulation time is 16 h in order to represent the relaxation phase. The results presented in Fig. 12 are based on Model 2 (without MS mechanism) and those in Fig. 13 are based on Model 3.

Figure 12a shows the simulated stress evolution at the surface and at the centre of the board during drying for a section located at the quarter span of the cantilever. After about one-half hour of drying, the moisture content at the wood surface drops below FSP (Fig. 4). With further drying, the surface attempts to shrink but is restrained by the interior of the beam which is still above FSP. This constrained state of deformation induces tensile stresses within the surface layers and compressive stresses in the center of the cantilever. After 2 h of drying, the tensile stress at surface reaches a maximum of 2.7 MPa and the compressive stress at the center reached a maximum of 0.8 MPa. These two maximum stresses are well below the plasticity threshold (Fig. 5). Towards the end stage of drying (8 h), a short stress inversion period is observed but the stresses are totally relaxed immediately after the drying is completed since the viscoplastic threshold was not reached. Figure 12b shows the stress profile through thickness at various drying times. It can be observed that much of the board section is under compressive stresses.

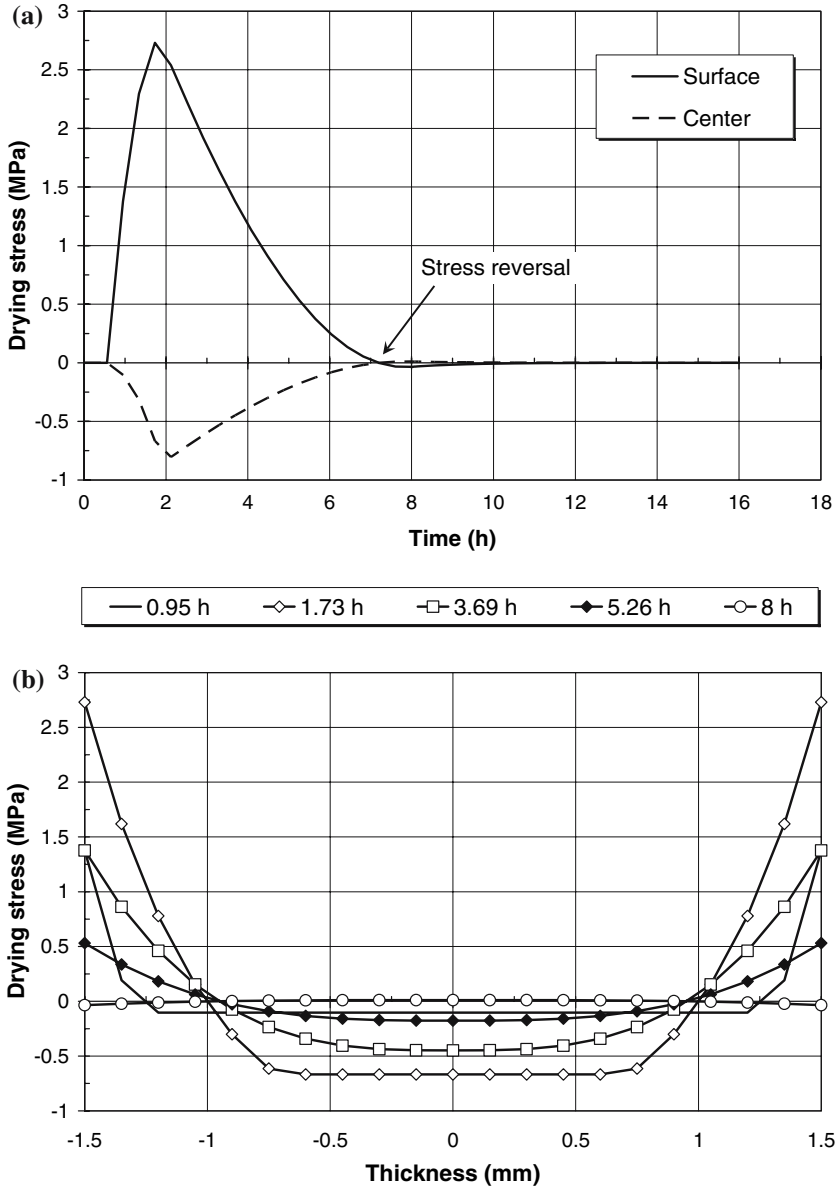

Fig. 12 Simulation results with Model 2 as applied to a cantilever at $x = l/4$ free of load during drying (real drying). **a** Stress at surface and center versus time. **b** Stress profile through thickness at different drying times

Examining the simulation results with the activated MS mechanism (Fig. 13), it can be seen that the maximum stress at the surface and in the core is lower than the one observed in Fig. 12a. Furthermore, the stress reversal phenomenon appears earlier in the drying process and a permanent residual

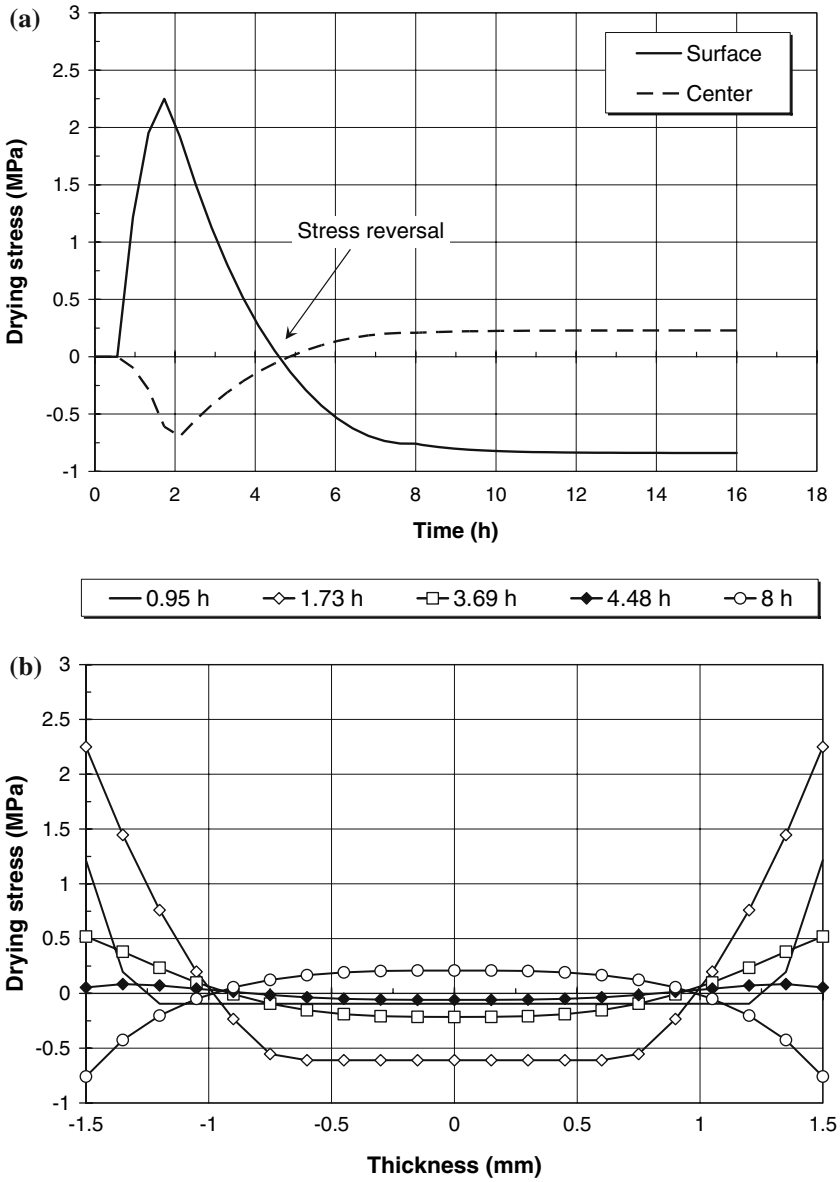

Fig. 13 Simulation results with Model 3 as applied to a cantilever at $x = l/4$ free of load during drying (real drying). **a** Stress at surface and center versus time. **b** Stress profile through thickness at different drying times

stress is present at the end of drying even if the plasticity threshold was not reached. This shows the importance of the conditioning treatment at the end of drying. If the MS mechanism contributes to decrease the risk of check formation at the surface in the beginning of drying, conversely it increases the level of residual stresses after drying for both the core and the shell. By

comparing Fig. 13b with Fig. 12b, we can also conclude that the mechano-sorptive effect has not much changed the stress profiles through thickness, except for the maximum values of the tensile and compressive stresses.

Conclusions

The objective of this study was to develop a rheological model of wood cantilever for modeling the creep behavior and stress in various moisture content conditions and various load levels. The following conclusions can be drawn from this work:

- In bending test configuration, the nonlinear stress due to the load level effect can be accurately predicted with the proposed elasto–viscoplastic model. The resolution of the strain and stress fields across the cantilever thickness does not rely on the hypothesis of linear stress distribution. Thus, the usual errors associated to the flexure creep tests are in great part eliminated.
- The cantilever beam configuration under load in constant or varying moisture content conditions allows simultaneous creep study in tension and in compression, and easy experimental identification of rheological model parameters.
- Classical viscoelastic rheological stress model is not sufficient to modeling drying stress in varying moisture content conditions. The mechano-sorptive effect must be considered in drying stress models even if the later has still not been fully understood.
- Drying stress simulation models can be used for the better understanding of the various viscoelastic and mechano-sorptive mechanisms which are difficult and cumbersome to study in the laboratory.

Work is ongoing to identify material properties of wood in radial oriented cantilever specimens and to modeling the transverse drying stresses in various moisture conditions.

Acknowledgments The authors are grateful for the financial support of this research from Natural Sciences and Engineering Research Council of Canada (No. 224297) and Forintek Canada Corp.

References

Allegretti O, Rémond R, Perré P (2003) A new experimental device for non-symmetrical drying tests. Experimental and numerical results for free and constrained samples. In: Proceedings of the 8th international IUFRO wood drying conference. Brasov, Romania, pp 65–70

Bingham EC (1922) Fluidity and plasticity. McGraw-Hill, New York

Dahlblom O, Petersson H, Omarsson S (2001) Full 3-D FEM-simulations of drying distortions in spruce boards based on experimental studies. In: Proceedings of the 7th international IUFRO wood drying conference. Tsukuba, Japan, pp 246–251

Dinwoodie JM, Paxton BH, Bonfield PW, Mundy JS (1995) Fatigue and creep in chipboard. Part 2. The influence of slow cyclic fatigue on the creep behavior of chipboard at a range of stress levels and moisture contents. Wood Sci Technol 29:64–76

Fortin Y, Naderi N, Laforest P, Cloutier A (1999) Viscoelastic and mechano-sorptive creep measurements of spruce wood in the longitudinal direction under kiln drying conditions. In: Proceedings of the 6th international IUFRO wood drying conference. Stellenbosch, South Africa, pp 225–226

Foudjet A, Bremond C (1989) Creep of four tropical hardwoods from Cameroon. Wood Sci Technol 23:335–341

Guitard D (1987) Mécanique du matériau bois et composites. Eds.; CEPADUES: Toulouse, France, 238 pp

Hanhijärvi A (2000) Deformation properties of Finnish spruce and pine wood in tangential and radial directions in association to high temperature drying. Part 3. Experimental results under drying conditions (mechano-sorptive creep). Holz Roh- Werkst 58:63–71

Haque MN, Langrish TAG, Keep LB, Keey RB (2000) Model fitting for visco-elastic creep of Pinus radiata during kiln drying. Wood Sci Technol 34:447–457

Kingston RST, Budgen B (1972) Some aspects of the rheological behavior of wood. Part 4. Non-linear behavior at high stresses in bending and compression. Wood Sci Technol 6:230–238

Mårtensson A (1994) Mechano-sorptive effects in wooden material. Wood Sci Technol 28:437–449

Mårtensson A, Svensson S (1997) Stress–strain relationship of drying wood. Part 1. Development of a constitutive model. Holzforschung 51:472–478

Miller DG, George P (1974) A method of measuring creep and recovery due to flexural loads of short duration. Wood Sci 7(2):153–159

Moutee M, Laghdir A, Fafard M, Fortin Y (2002) A three-dimensional mathematical model of the hygro-thermo-mechanical behavior of wood during drying. In: Proceedings of forest product society conference ''Quality Drying: The Key to Profitable Manufacturing''. Montreal, Canada, pp 179–184

Moutee M, Fafard M, Fortin Y, Laghdir A (2005) Modeling the creep behavior of wood cantilever loaded at free end during drying. Wood Fiber Sci 37(3):521–534

Ormarsson S, Dahlblom O, Petersson H (1999) A numerical study of the shape stability of sawn timber subjected to moisture variation. Part 2. Simulation of drying board. Wood Sci Technol 33:407–423

Pang S (2001) Modeling of stresses and deformation of Radiata Pine lumber during drying. In: Proceedings of the 7th international IUFRO wood drying conference. Tsukuba, Japan, pp 238–245

Perré P, Passard J (2004) A physical and mechanical model able to predict the stress field in wood over a wide range of drying conditions. Dry Technol 22(1–2):27–44

Ranta-Maunus A (1990) Impact of mechano-sorptive creep to the long-term strength timber. Holz Roh-Werkst 48:67–71

Ranta-Maunus A (1992)Determination of drying stress in wood when shrinkage is prevented: test method and modeling. In: Proceedings of the 3rd international IUFRO wood drying conference. Vienna, Austria, pp 139–144

Ranta-Maunus A (1993) Rheological behaviour of wood in directions perpendicular to the grain. Mater Struct 26:362–369

Rice RW, Youngs RL (1990) The mechanism and development of creep during drying of red oak. Holz Roh-Werkst 48:73–79

Salin JG (1989) Prediction of checking, surface discoloration and final moisture content by numerical methods. In: Kayihan F, Johnson JA, Smith WR (eds) Upgrading wood quality through drying technology. International Union of Forestry Research Organisations, Washington, pp. 222–225

Salin JG (1992) Numerical prediction of checking during timber drying a new mechano-sorptive creep model. Holz Roh-Werkst 50:195–200

Shames IH, Cozzarelli FA (1992) Elastic and inelastic stress analysis. Prentice-Hall, Englewood Cliffs, New Jersey

Svensson S (1995) Strain and shrinkage force in wood under kiln drying conditions. Part 1. Measuring strain and shrinkage under controlled climate conditions. Equipment and preliminary results. Holzforschung 49(4):363–368

Svensson S (1996) Strain and shrinkage force in wood under kiln drying conditions. Part 2. Strain, shrinkage and stress measurements under controlled climate conditions. Equipment and preliminary results. Holzforschung 50(5):463–469

Wu Q, Milota MR (1995) Rheological behavior of Douglas-fir perpendicular to the grain at elevated temperatures. Wood Fiber Sci 27(3):285–295

Wu Q, Milota MR (1996) Mechano-sorptive deformation of Douglas-Fir specimens under tangential tensile stress during moisture adsorption. Wood Fiber Sci 28(1):128–132